International Journal of Nanoelectronics and Materials
Volume 15, No. 3, July 2022 [223-232]

Aggregation threshold for Novel Au – $LiNbO_3$ core/shell Nano composite: effect of laser ablation energy fluence

Marwa. S. Alwazny[1, 2*], Raid. A. Ismail[1], Evan. T. Salim[1]

[1]Department of Applied Science, University of Technology-Iraq.
[2]Laser and Optoelectronics Engineering Department, University of Technology-Iraq.

Received 6 February 2022, Revised 9 April 2022, Accepted 20 April 2022

ABSTRACT

In this paper, unique nanocomposites of Gold: Lithium Niobate (Au-$LiNbO_3$) were synthesized for the first time utilizing pulse laser ablation in liquid method (PLAL). Q-switched neodymium-*doped yttrium aluminum garnet (Nd: YAG) laser was used to prepare suspension at different laser fluence in water environment for LN and Au targets, then deposited at n-Type silicon substrates. XRD analysis used to define the structure nature of these films. Photoluminescence measurements exhibited distinct emissions peaks that decreased as the laser fluence escalated. The surface morphology was examined using field emission scanning electron microscopy (FESEM) and transmission electron microscopy (TEM), while image j software was used to determine surface nature and particles size of Au- $LiNbO_3$ thin films. It is found aggregation threshold decrease as laser fluence increases with zeta potential ranging about -16 to -12 mV..*

Keywords: aggregation threshold; Core shell; LN-Au; laser fluence, Zeta potential.

1. INTRODUCTION

Lithium niobate ($LiNbO_3$) is considered one of the most intensively researched semi insulator material used to fabricate thin film, due to the excellent physical and nonlinear properties suitable for variety of optical and photonic applications [1], The spotlight in the electronics industries has evolved from bulk LN to producing $LiNbO_3$ thin films at a nanoscale with low optical loss, which will allow to reintroduce them into fully established Si-based semiconductor technology. [2-4].

It has been demonstrated that the LN characteristics could be enhanced by insertion of additives [5, 6], thus many researchers attempt to prepare heteroepitaxial nanomaterial based on $LiNbO_3$ nanoparticles, such as Nd-doped $LiNbO_3$ films reported by J. E. Alfonso et. al. [5], Mg-doped $LiNbO_3$ reported by A.Z. Simo˜ es et al. [4] and Sc_2O_3 and Lu_2O_3 doped $LiNbO_3$ reported by Anil Tumuluri et. al. [7]. Species sizes, particles shapes, crystal facets, structure, and composition that are precisely determined could be routinely synthesized and controlled depend on growth techniques such as spray pyrolysis [8], metal organic chemical vapor deposition (MOCVD) [9], spin coating [10, 11], molecular beam epitaxy (MBE) [12], sol–gel [13, 14] , and PLD [15-17].

To our knowledge, no researchers have attempted to synthesize $LiNbO_3$ as core-shell nanomaterial using laser ablation in liquid. Zeta potential or electro kinetic potential is defined as the difference in the potential between shear plane of colloidal particles and the electro neutral region of dispersion solution.
Since zeta potential indicates the degree of electrostatic repulsion between two adjacent and similarly charge particles, it is considered as the key indicator of the stability of colloidal

*Corresponding author: marwa.s.mohsin@uotechnology.edu.iq

dispersion [18] since it is used to demonstrate colloidal stability starting from rapid coagulation of the particle or when the aggregation threshold leads to the beginning formation of contiguous clusters of colloidal particles up to different levels of stable particle [19].

In this paper, we will synthesize an Au – LN nanocomposite to improve the properties of $LiNbO_3$ as heterogeneous nanocomposite material, including special metals like Au, which often assists as dynamic catalytic component [20]. The main advantages of core-shell nanoparticles are (1) because of the shell material coating, properties of the core material such as reactivity can be decreased and thermal stability can be modified, so that the overall particle stability and dispensability of the core particle increases, and (2) the shell material can provide surface chemistry for further modification and functionalization of the nanoparticles. In addition, these types of morphology give advantages for photodetector devices through broadening the spectrum of detection as well as enhancing the properties of photodetector via reducing the electron-hole recombination.

Our attempt to synthesis $LiNbO_3$ composite with noble metal nanomaterial built with Nano cores made of gold and LN acting as nanoshells will be defined as CSNs (core–shell nanoparticles). Then we concentrate on the effect of laser fluencies on prepared samples and aggregation threshold throughout zeta potential.

2. EXPERIMENTAL WORK

Au colloidal nanoparticles were prepared using pulsed laser ablation in liquid technique (PLAL), where an Au pellet was irradiated with the 532 nm of a Q-switched Nd: YAG laser functioning at 1 Hz, 480 mJ laser energy, 70 laser pulse and 2 mm laser spot size of 2 mm, immersed in 3 ml of water. A $LiNbO_3$ Z-cut wafer was consequently placed in Au colloidal then shot by 200 laser pulse at different laser fluencies of 1.3, 1.6, 2, and 2.2 J/cm^2. N-type silicon was used as a substrate for CSNs Au-LN deposition. To analyze structural qualities, an X-Ray Diffractometer (Panalytical X' Pert Pro) was employed. FESEM of (ZEISS SEGMA VP) was used to identify the morphology, while Image J software was used to conclude the particle size distribution. Suspension stability was determined and evaluated using a zeta potential (Malvern Zeta sizer) device.

3. RESULTS AND DISCUSSION

$LiNbO_3$ commonly exhibits remarkable photoluminescence (PL) features – strong and widely distributed in bands of emission in the UV-Visible area. Photoluminescence (PL) of Au – $LiNbO_3$ CSNs presented in Fig 1 (a) exhibited distinct emissions peaks at 343, 345, 340, 335, 420 and 510 nm for 1.3, 1.6, 2, and 2.2 J/cm^2 laser fluence, respectively. The sustained emission band approaching 510 nm, indicating that the anti-site defectNb_{Li}^{4+} which means that Nb^{4+} ions are positioned in Li- sites. The occurrence of the photoluminescence peak in reduced crystals and in samples depleted of Li due to heat impact or changes in the Li:Nb stoichiometry supports this theory [9, 21] and in our case, by laser fluence. Fig 1 (b) shows a magnified view of the peaks; it is common to see an intrinsic emission blue band at 400 nm in stoichiometric $LiNbO_3$, which appears to be unrelated to the excitation wavelength of 250 nm. Indeed, this band was seen in both pure and doped $LiNbO_3$, and it is developed as a result of intrinsic electron (Nb^{4+}) and hole (O^-) recombination at the niobate group [22]. Although this peak is small, it is still appeared at higher laser fluence at 420 nm. It is well known that the recombination efficiency is the basic factor that controls the PL peak intensity and height, as laser fluence escalated, PL intensity shrink (slow rate electron-hole pair recombination). This may attribute to the shell thickness growing and change of CSNPs size.

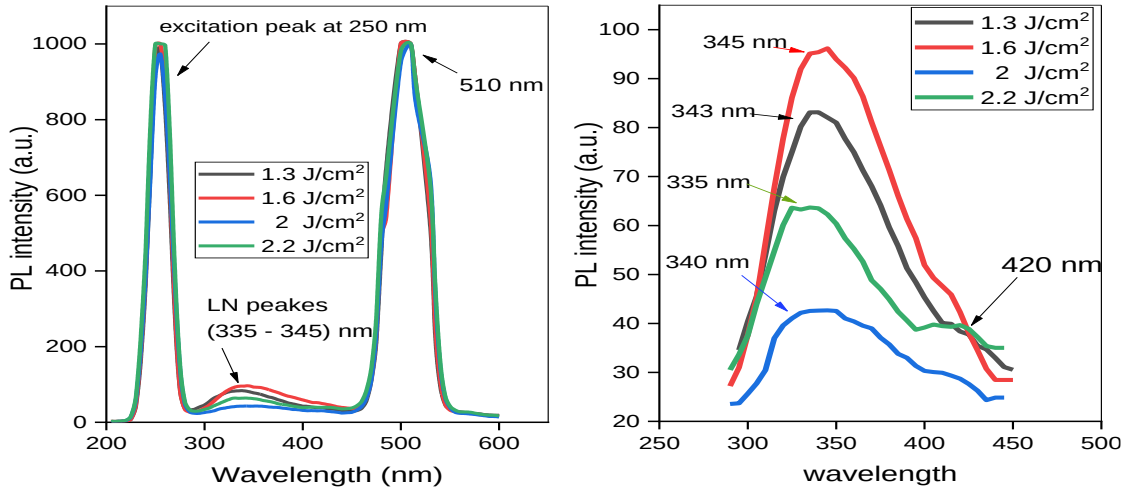

Figure 1. (a) PL spectra for the LN at different laser fluence, **(b)** magnified view of the peaks at (345-335) nm

In this study, energy gap values for Au – LN CSNs from PL is calculated using the following equation [23, 24] :

$$Eg = 1240/\lambda \quad (1)$$

where λ is the emission peak. . Fig. 2(a) shows the calculated energy gap from PL peaks and it comparison with UV Vis results at different laser fluencies. An increase in energy gap occurs with decreased laser fluencies, where PL energy gap almost matches the UV-Vis results. PL spectra of Au-LN nanocomposite shows peaks at (343, 345, 340, and 353) nm and corresponding to (1.3, 1.6, 2, and 2.2) J/cm² laser fluences, and the results show a slight blue shift with increasing laser fluence. This may attribute to the change in CSNs size as presented in FESEM and TEM results. This shift is as illustrated in Fig. 2 (b).

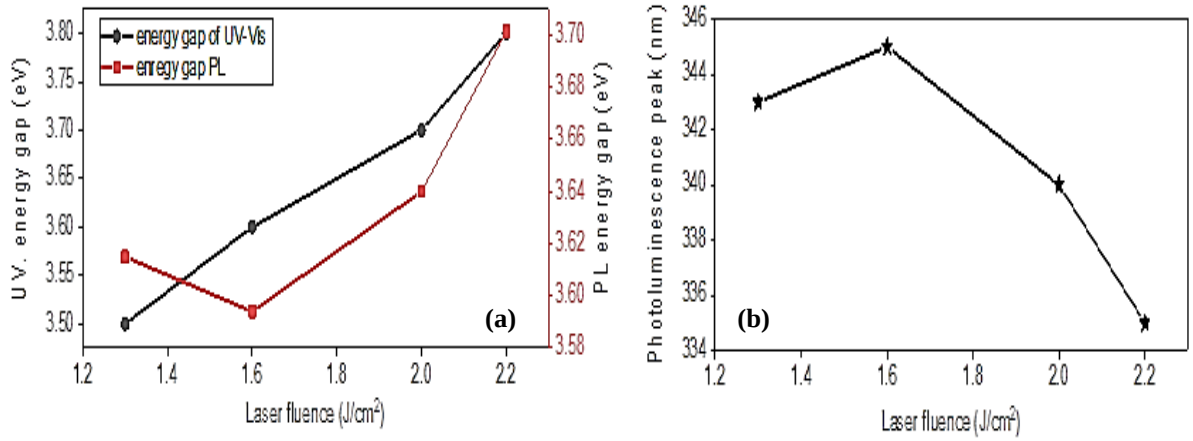

Figure 2. (a) energy gap extracted from UV-Vis and PL at different laser fluencies, (b) is the change in peak shifts with different laser fluencies

It would be more preferable to grow Au – $LiNbO_3$ on silicon substrate because this will make it feasible to construct optical devices or to explore structural and morphological properties [1]. Thus the crystalline structure examined by XRD of $LiNbO_3$, which known to be hexagonal

structure and have ferroelectric phases of space group R3c of trigonal symmetry with ten atoms per unit cell, given vast range of LN applications as presented in the inset in Fig 3. XRD analysis of the hybrid Au - $LiNbO_3$ core shell is shown in Fig 3. All diffraction peaks have been identified as arising due to the presence of lithium niobate $LiNbO_3$ and Au. The Standard Bragg reflection peak of face center cubic (fcc) lattice related to Au can be seen at 44.5^0, 66^0 of (200, 220) plane appeared at all samples prepared at different laser fluence, while sample prepared at 1.6 J/cm^2 showes another small peak of Au at 38.4^0 corresponding to (111), where similar peak of Au nanoparticles reported by other literature [24, 25]. Similarly, $LiNbO_3$ shows peaks at 33^0, 47^0, 54^0, 56^0 and 61^0 corresponding to (104), (024), (116), (122), and (214) respectively. Laser fluence of 1.3, 2 J/cm^2 showed a small peak at 57.4^0 at (018) plane. The Au - LN structure enhanced with increased laser fluence except for sample prepared at 1.6 J/cm^2. This may be attributed to changes in the particle size and core structure.

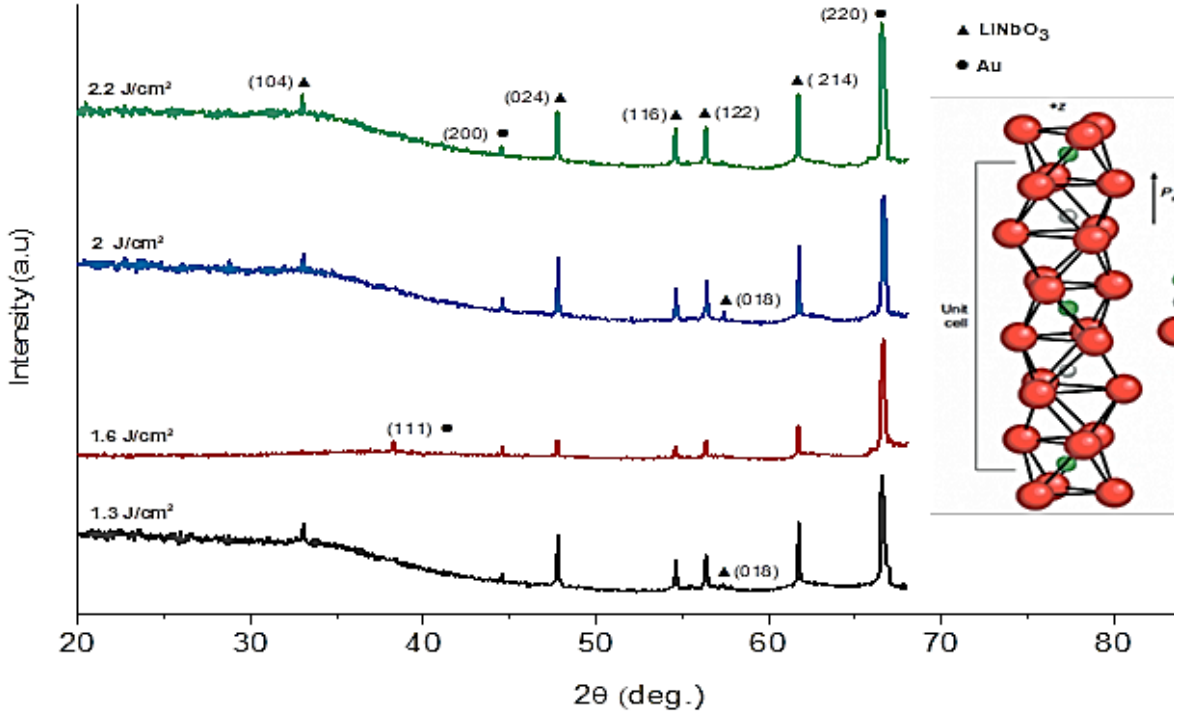

Figure 3. XRD analysis of Au-LN nanoparticles prepared at different laser fluencies. [inset] crystalline structure of $LiNbO_3$ [24, 25]

Surface morphology of the prepared Au – LN thin films is shown in Fig 4. The result shows grain size about 34, 26.8, 21.8 and 13.4 nm for laser fluence of 1.3, 1.6, 2, 2.2 J/ cm^2 respectively (particles size determined by image J software). Samples prepared at 1.6-2.2 J/cm^2 show uniform and dense structure, and defined particles at 2 J/cm^2 then at 2.2 J/cm^2 film show more dense with merge particles boundary. Surface morphology for these samples show increase in aggregation with increasing laser fluence.

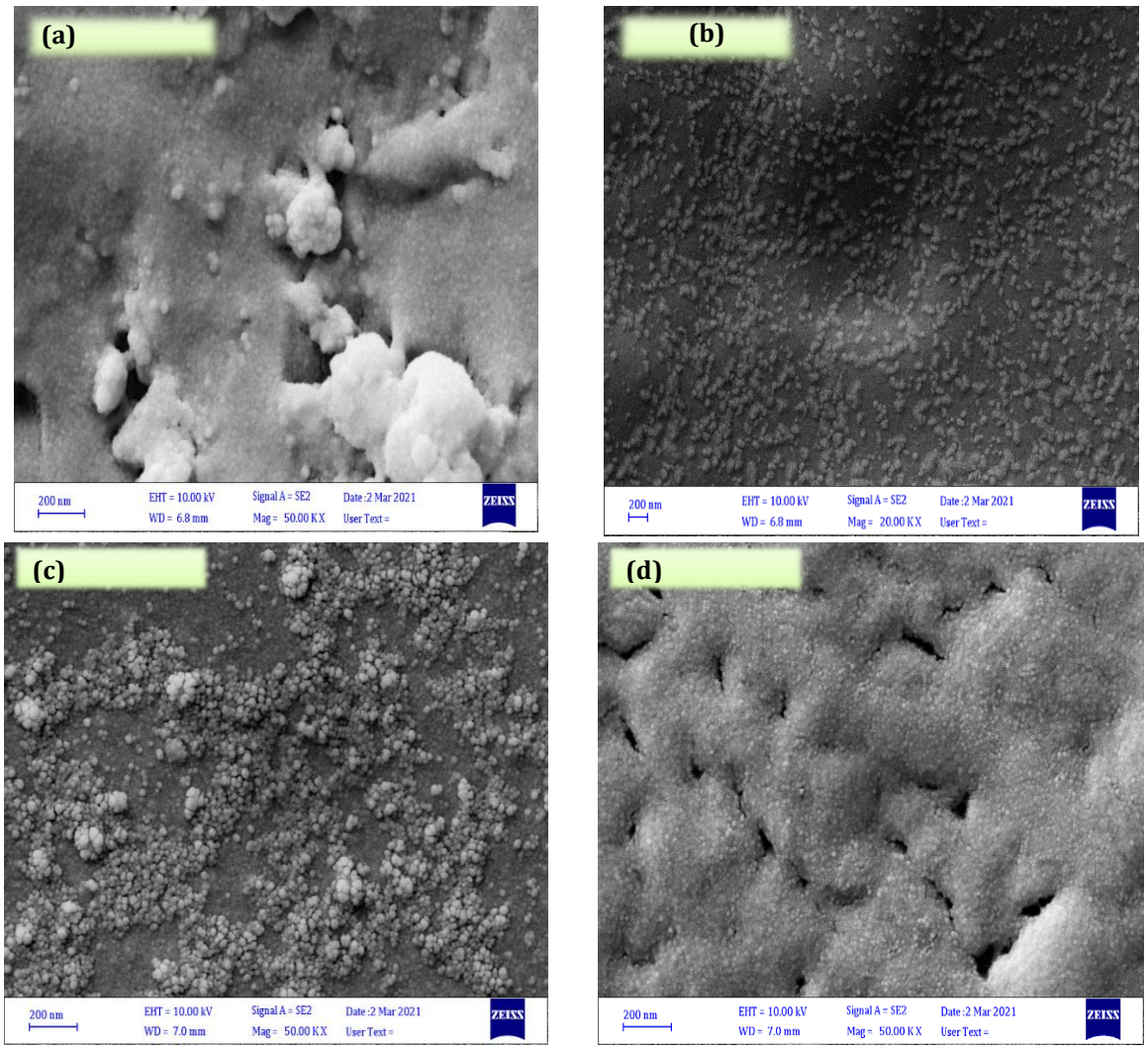

Figure .4. SEM images for Au – $LiNbO_3$ prepared at (a) 1.3 J/cm^2, (b) 1.6 J/cm^2, (c) 2 J/cm^2, and (d) 2.2 J/cm^2

TEM image for Au – LN core shell colloidal at different laser fluence is shown in Fig. 5. The results support the decrease in particle size suggested in the PL and FESM results and also in the incoming zeta potential results, whereas laser fluence increases, more stable colloidal and less aggregation occurs.

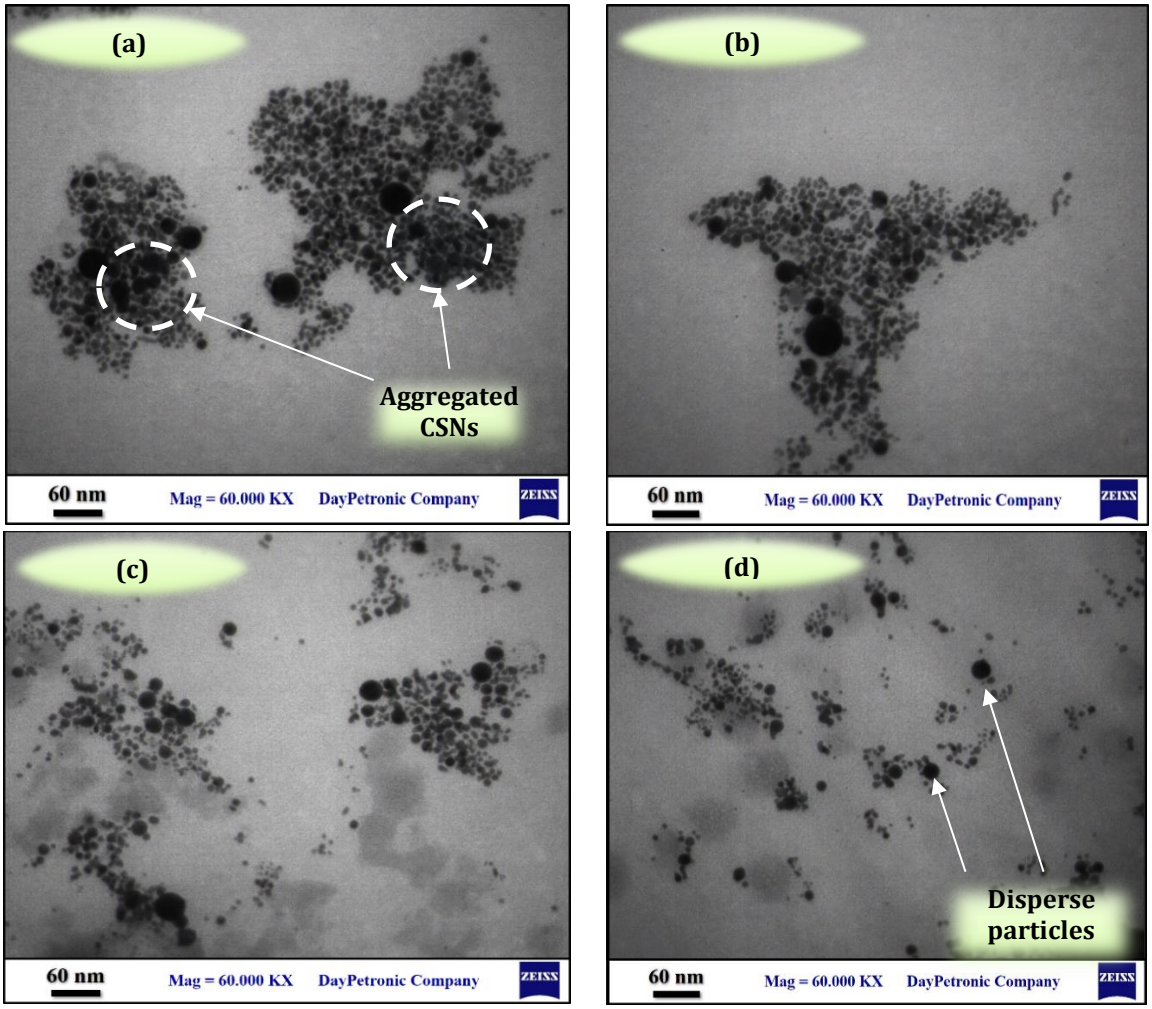

Figure 5. TEM images of Au - $LiNbO_3$ suspension in deionized water at different laser fluence of: (a) 1.3 J/cm^2, (b) 1.6 J/cm^2, (c) 2 J/cm^2, and (d) 2.2 J/cm^2

The zeta potential (ZP) of hybrid Au-LN nanocomposite particles was evaluated using the Zetasizer Ver. 6.01 instrument to assess particle suspension stability. According to Smoluchowski's equation, the equipment determines electrophoretic mobility (U) and ZP automatically [26]:

$$\xi = \frac{U\eta}{\varepsilon} \qquad (2)$$

where ξ is the ZP, η the medium viscosity, U the electrophoretic mobility, and ε is the dielectric constant.

In general, the zeta potential is just the difference in electrical potential between both the dispersion surrounding the dispersed particle and the immobile layer of liquid associated with it. It is important because it may correlate to particle dispersion stability. A strong ZP, either negative or positive in quantity, confers suspension fastness, i.e., the particles withstand aggregation and agglomeration for molecules and particles that are small enough. Once the potential is minimal, attraction exceeds repulsion, resulting in the clustering of the particles. As a result, particles with an elevated ZP are electrically settled, whereas species with a minimal ZP curd or flocculate, as shown in Table 1 [27, 28], and illustrated in Fig 6.

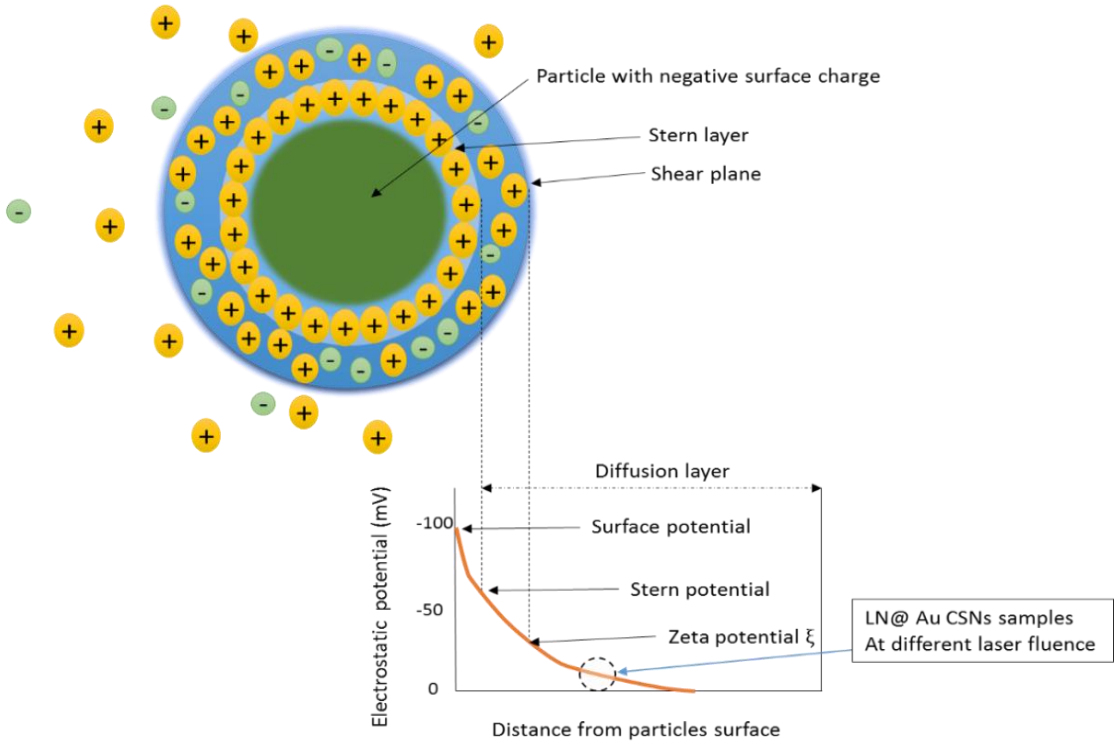

Figure 6. Schematic diagram of zeta potential for nanoparticles in suspension

Table 1. The relation between zeta potential and particles stability [26].

Zeta potential [mV]	Stability behavior of the particle
0 to -5	Rapid coagulation or flocculation
-11 to -30	Incipient instability (threshold of agglomeration)
-30 to -40	Moderate stability
-40 to -60	Good stability
More than -61	Excellent stability

According to Derjaguin and Landau, Verwey and Overbeek (DLVO) theory, [28-30], the total interparticle potential is equal to the sum of Van der Waals attractive and repulsive energy. A significant electromagnetic field created by near-field light enhancement can modify surface charge distribution, influencing interparticle potential and suspension stability. As a result, it is proposed that the electrostatic charge on the suspension's surface should change with laser power over the area; however, the granules in the suspension lighted with relatively low laser fluence agglomerated more due to limited electrostatic surface charge, which is responsible for repulsive forces. As a result, establishing high and long-term stability with respect to mean particle dispersion is critical, as is increasing the laser fluence to an appropriate level. Thus, a wide range of laser fluence was needed to set the optimal value as illustrated in Fig 7.

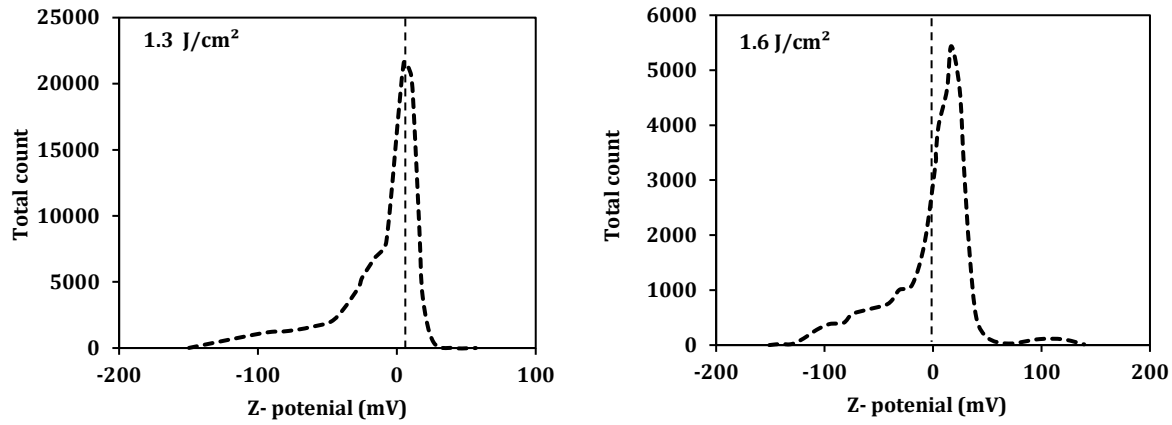

Figure 7. Zeta potential for suspensions prepared at different laser fluencies fluences of (a) 1.3 J/cm^2, (b) 1.6 J/cm^2, (c) 2 J/cm^2, and (d) 2.2 J/cm^2.

In our case, zeta potential increase with increased laser fluence mean decrease in aggregation. This may also be related to the decrease in particle size as presented by other researchers [29, 31], which can be seen in Fig. 8**,** where CSNs mobility and stability increase with increasing laser fluencies.

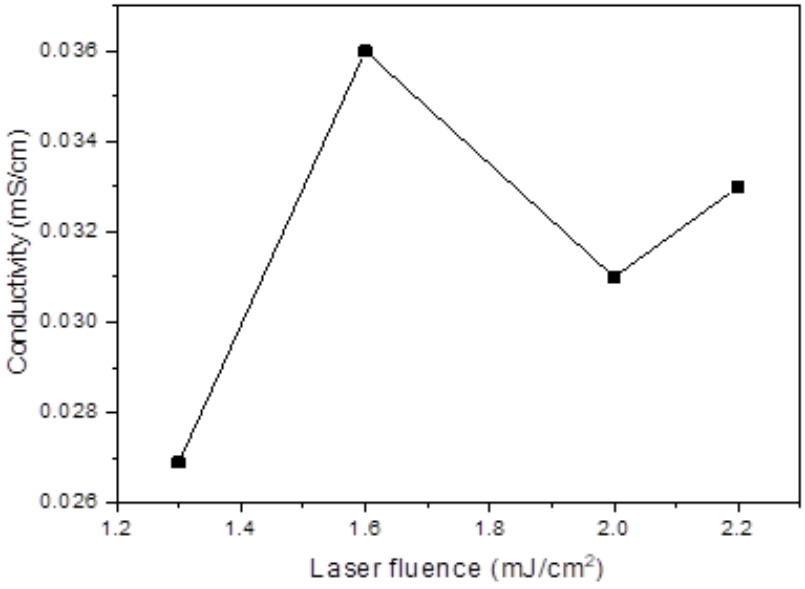

Figure 8. Au-LN conductivity at different laser fluencies**.**

4. CONCLUSIONS

In this paper, the structure of Au – $LiNbO_3$ thin films deposited at n-type silicon show a decrease in particle size and energy gap from (34, 26.8, 21.8 and 13.4) nm and (3.5-3.8) eV respectively. Known peaks for both LN and Au refer to the growth of polycrystalline structure for Au-LN nanocomposite. The increase in laser fluencies lead to more stable suspension and less aggregation, although all samples are in the threshold of aggregation where zeta potential values range about (-16 to -12) mV. This may related to the change in particles size and surface to volume ratio and thus, the charge existence on surface.

REFERENCES

[1] Wang, X., Ye, Z., He, J., Cao, L., Zhao, B., Mater. Lett., vol **58**, (2004) pp. 3597–3600.
[2] W. C. Shih, T. L. Wang, X. Y. Sun, and M. S. Wu, Jpn. J. Appl. Phys., vol **47** (2008) pp. 4056–4059.
[3] Mohammed, L.Z., Fakhri, M.A., Abass, A.K.,, Journal of Physics: Conference Series, vol **1795** issue1, (2021) pp. 012055
[4] Simões, A. Z., González, A. H. M., A. A. Cavalheiro, M. A. Zaghete, B. D. Stojanovic, and J. A. Varela, Ceram. Int., vol **28** (2002) pp. 265–270.
[5] Alfonso, J. E., Martín, M. J., Zaldo, C.., Appl. Phys. Lett., vol **71** (1997) pp. 2904–2906.
[6] Fakhri, M. A., AbdulRazzaq, M. J., Alwahib, A. A., Muttlak, W. H., Optical Materials, vol **109** (2020) pp. 110363
[6] Simões, A. Z., Gonzalez, A. H., Riccardi, C. S., Cilense, M., Zaghete, M. A., Stojanovic, B. D., Tangastev, A., Setter, N., Varela, J. A., Integr. Ferroelectr, vol **43** (2002) pp. 123–135.
[7] Tumuluri, A. Raju, K. C. J., Ceram. Int., vol **40** (2014) pp. 3371–3377.
[8] Fakhri, M. A., Salim, E. T., Wahid, M. H. A., Hashim, U., Salim, Z. T., J. Mater. Sci. Mater. Electron., vol **29** (2018) pp. 9200–9208.
[9] Feigelson, R. S., Cryst. J., Growth, vol. **166** (1996) pp. 1–16.
[10] Al-Douri, Y., Fakhri, M. A., Badi, N., Voon, C. H., Optik, vol **156** (2018) pp. 886–890.
[11] Faisal, A. D., Ismail, R. A., Khalef, W. K., Salim, E.T., Optical and Quantum Electronics, vol **52** (2020) pp. 1-12.
[12] Betts, R. A. Pitt, C. W., Electron. Lett., vol **21** (1985) pp. 960–962.
[13] Fakhri, M. A. , Al-Douri, Y., Hashim, U., Salim, E. T., Sol. Energy, vol **120** (2015) pp. 381–388.
[14] Abood, M., Salim, E. T., Saimon, J. A., Journal of Ovonic Research, vol **15** issue 2 (2019) pp. 109 – 115
[15] Kim, H. J., Kim, D., Ha, J., Kang, C., Sung, M. Y., Cho, B. H., Yoon, S., Kim H., J. Electroceramics, vol **17** (2006) pp. 933–935.
[16] Salim, E. T., Al-Douri, Y., Al Wazny, M. S., Fakhri, M. A., Sol. Energy, vol **107** (2014) pp. 523–529.
[17] Al-Douri, Y., Fakhri, M. A., Bouhemadou, A., Khenata, R., Ameri, M., Materials Chemistry and Physics, vol **203** (2018) pp. 243-248.
[18] Honary, S., Zahir, F., Trop. J. Pharm. Res., vol **12** (2013) pp. 255–264.
[19] M. B. Gawande, Goswami, A., Asefa, T., Guo, H., Biradar, A. V., Peng, D., Zboril, R., Varma, R. S., Chem. Soc. Rev., vol **44** (2015) pp. 7540–7590.
[20] Fakhri, M. A., Al-Douri, Y., Salim, E. T., Hashim, U., Yusof, Y., Choo, E. B., Salim, Z. T., Jurn, Y. N., ARPN Journal of Engineering and Applied Sciences, vol **11** issue 8 (2016) pp. 4974-4978
[21] Blasse, G., Haart, L. G. J. D., Mater. Chem. Phys., vol **14** (1986) pp. 481–484.
[22] Fakhri, M. A. Salim, E. T., Wahid, M. H. A., Hashim, U., Salim, Z. T., J. Mater. Sci. Mater. Electron., vol **29** (2018) pp. 9200–9208.
[23] Krishnamurthy, S., Esterle, A., Sharma, N. C., Sahi, S. V., Nanoscale Res. Lett., vol **9** (2014) pp. 1–9.
[24] Mamoun, S., Merad, A. E., Guilbert, L., Comput. Mater. Sci., vol. **79** (2013) pp. 125–131.
[25] Taleb, S. M., Fakhri, M. A., Adnanm, S. A., Defect and Diffusion Forum, vol **398** (2020) pp. 16-22
[26] Doostmohammadi, A., Monshi, A., Salehi, R., Ceram. Int., vol **37** (2011) pp. 2311–2316.
[27] Taleb, S. M., Fakhri, M. A., Adnan, S. A., Journal of Ovonic Research, vol **15** issue 4 (2019) pp. 261-269
[28] Seo, Y., Choi, T. Y., Ha, J., Jeong, D. Y., Lee, S. Y., Kim, D., J. Appl. Phys., vol **118** (2015) pp. 11.
[29] Mohsin, M. H., Ismail, R. A., Mhadi, R. O., Appl. Phys. A Mater. Sci. Process., vol. **127** (2021) pp. 1–10.
[30] Fakhri, M. A., Al-Douri, Y., Bouhemadou, A., Ameri, M., Journal of Optical Communications, vol **39** issue 3 (2017) pp. 297-306
[31] Ismail, R. A., JSTS., vol. **9** issue1 (2009) pp. 51-54.